Processing and Application of Ceramics 14 [4] (2020) 282–292
https://doi.org/10.2298/PAC2004282M

Crystalline WO_3 nanoparticles for NO_2 sensing

Branko Matović[1,*], Jelena Luković[1], Dejan Zagorac[1], Olga S. Ivanova[2], Alexander E. Baranchikov[2,3], Taisiya O. Shekunova[2,3], Khursand E. Yorov[2,3], Olga M. Gajtko[2], Lili Yang[3], Marina N. Rumyantseva[3], Vladimir K. Ivanov[2,3,4]

[1]*Vinča Institute of Nuclear Sciences, University of Belgrade, Belgrade, Serbia*
[2]*Kurnakov Institute of General and Inorganic Chemistry of the Russian Academy of Sciences, Moscow, Russia*
[3]*Lomonosov Moscow State University, Moscow, Russia*
[4]*National Research Tomsk State University, Tomsk, Russia*

Received 16 April 2020; Received in revised form 27 July 2020; Accepted 31 August 2020

Abstract

This study shows excellent NO_2-sensing properties of tungsten oxide nanoparticles, prepared using a facile procedure which includes dissolution of metallic tungsten in hydrogen peroxide with subsequent low-temperature (400 °C) heating. We also conducted a thorough literature survey on sensor properties of tungsten oxide prepared by various means and found that the sensor response towards NO_2 registered in this work achieved the highest level. The most intriguing feature of the material obtained was a highly reproducible sensor signal at room temperature which was more than 100 times higher than any reported previously for WO_3. The probable reason for such high sensor response was the presence of two WO_3 polymorphs (γ-WO_3 and h-WO_3) in the material synthesized using a peroxide-assisted route. In order to further investigate synthesized WO_3 materials, sophisticated experimental (XRD, SEM, TEM, BET) and theoretical (B3LYP, HSE) methods have been used, as well as resistance and sensor response measurements at various temperatures.

Keywords: *tungsten oxide, polymorph, sensor properties, NO_2, ab initio*

I. Introduction

Tungsten oxide (WO_3) is a wide band gap semiconductor with a bandgap varying from 2.7 to 3.15 eV, depending on the oxygen vacancy concentration [1]. Tungsten oxide is widely used in solar cells [2], supercapacitors [3] and photochromic [4], gas chromic [1] and electrochromic [5] devices, humidity sensors [6], and as a photocatalyst for enhanced water splitting [7] and water purification [8–10]. Special attention is currently paid to the sensing properties of WO_3. Pure WO_3, as well as loaded/doped WO_3 [11], is used for the detection of both organic (trimethylamine [12], ethanol [13], methanol and formaldehyde [14], and acetone [15]) and inorganic (H_2 [16], H_2S [17], NH_3 [18], NO [19]) gases. WO_3 demonstrates the highest sensitivity and selectivity towards NO_2, over a wide range of temperatures [20,21]. It has been repeatedly shown that the sensing properties of WO_3 are affected by several key parameters, including phase composition [22], microstructure [23–25], temperature of annealing [26] and visible light illumination [27]. Functional characteristics of tungsten oxide are largely determined by synthesis method, therefore, new approaches to WO_3 synthesis, or significant modification of existing ones, still remain the most crucial task. The most often methods used for WO_3 synthesis are hydrothermal [3,4,10,11,13,23,28–32] and solvothermal [19,22,24,25,33] methods, sol-gel technique [27,34–37] and spray pyrolysis method [21,38,39]. There are also a few reports concerning WO_3-based NO_2 sensors prepared by precipitation [12,40–42], gas transport [20], thermal decomposition [18], thermal oxidation [43] or high temperature anodization of metallic tungsten [16], electrospinning [44] and low frequency electrophoretic deposition [45]. Most of these methods are multistage and time-consuming.

A great deal of attention is currently paid to the design of sensor materials with good sensor properties by engineering various composites [46,47]. The enhance-

*Corresponding author: tel: +381 649271109,
e-mail: *mato@vin.bg.ac.rs*

ment of sensor properties in the composites is achieved by creating a junction of several phases with different conduction band levels. Generally, the synthesis of such composites is a much more complex task than the synthesis of individual compounds, requiring additional stages. Tungsten(VI)-oxide is a unique substance, which can exist in numerous polymorphs (having a ReO_3-type or hexagonal bronze structure) with different electronic properties [48,49]. By varying synthesis conditions within a single synthesis approach, one can easily obtain two-phase composite materials containing several WO_3 polymorphs as reported in the literature [50], thus achieving good sensor properties inherent to traditional composites. To the best of our knowledge, this idea in regard to the design of the sensor materials has not previously been discussed in the literature. In this paper, we report on WO_3 synthesis by a facile hydrogen peroxide-assisted procedure that we have described earlier [51], for highly sensitive NO_2 detection. This synthetic route gives a material with a highly reproducible sensor signal at room temperature, which is more than 100 times higher than any reported previously for a single-phase WO_3.

II. Experimental

2.1. Synthesis

Metallic tungsten (Koch-Light Laboratories, LTD, purity 99.9%, average grain size of 1 μm, according to the manufacturer's specification), hydrogen peroxide (Sigma-Aldrich) and 2-propanol (Sigma-Aldrich) were starting materials for the synthesis of WO_3 powder. All chemicals were used without further purification.

Tungsten(VI)-oxide was prepared by dissolving 5 g of elementary tungsten in a previously prepared mixture of 50 ml of 30 wt.% H_2O_2 solution, 5 ml of 2-propanol and 10 ml of H_2O. The reaction was very rapid; it took less than a couple of minutes, at room temperature, for dark-grey tungsten powder to turn into white powder formed in the reaction mixture. After decanting a liquid, and drying the residue overnight at 80 °C in the air, a yellowish WO_3 powder was obtained. This method for the synthesis of WO_3 nanoparticles for tungsten carbide (WC) composite preparation was described by Hepel and Hazelton [52]. In-depth investigations of the properties of tungsten(VI) oxide thus prepared were not conducted. The additional annealing of WO_3 powder was carried out in a muffle furnace at 400 °C in the air in an alundum crucible for 2 h.

2.2. Characterization

Powder X-ray diffraction (XRD) analysis of the samples was performed on a Bruker D8 Advance diffractometer (Bragg–Brentano geometry) with Ni-filtered CuKα radiation and a LYNXEYE detector. Diffraction patterns were recorded in the 10–70° 2θ range, with a step of 0.02° and collection time of 0.3 s/step. Phase identification was carried out with reference to the JCPDS PDF2 database using Crystallographica Search-Match software [53].

The microstructure of the samples was investigated using a Carl Zeiss NVision 40 high resolution scanning electron microscope at 1–7 kV acceleration voltage and a Leo912 AB Omega transmission electron microscope at 100 kV accelerating voltage.

The values of specific surface area were determined by low-temperature nitrogen adsorption on a Katakon ATX-06 analyser, using the 5-point Brunauer-Emmett-Teller model (BET) in the range of partial nitrogen pressures of 0.05–0.25. Before the measurements, samples were degassed in a dry helium flow at 200 °C for 30 min.

Sensing properties of the synthesized WO_3 powder towards NO_2 gas were determined by *in situ* measurements of the electrical conductivity of thick films. WO_3 powder was mixed with a binder (α-terpeniol in ethanol) and deposited as a paste onto a microelectronic chip with a platinum heater and electrodes. The films were annealed at 300 °C for 3 h, to remove the binder. Electrical conductivity was measured in situ in a flow cell (100 ml) under the conditions of a controlled gas flow of 100 ± 0.1 ml/min. The gas mixtures containing 0.1–2.0 ppm NO_2 in the air were prepared by diluting the certified gas mixture (20 ppm NO_2 in nitrogen) with a dry synthetic air using electronic Bronkhorst gas flow controllers. The measurements (15 min in the presence of NO_2 and 30 min in a pure dry air) were carried out at a constant current in the stabilized voltage mode (U = 1 V). The heaters were powered using an Agilent 6448 precision power source.

2.3. Computational details

The *ab initio* calculations were performed with the CRYSTAL17 code, a well-established computational tool for solid state chemistry and physics based on local Gaussian type orbitals [54]. Structure optimizations, band structure and density of states (DOS) calculations were performed using hybrid HSE (Heyd-Scuseria-Ernzerhof) and B3LYP (Becke's three parameter functional in combination with the correlation functional of Lee, Yang and Parr) functional, in order to describe electronic exchange and correlations [55,56]. For the *ab initio* calculations, a [4*s*3*p*] all-electron basis set was used for oxygen as in Refs [57–59]. For tungsten, the [4*s*4*p*2*d*] effective core pseudopotential was used as in Refs [60,61], and it was especially important to obtain the proper band structure and band gap of WO_3 [62–65] (further details are presented in the Supporting Information[§]). The tolerances for the convergence on energy were set to 1.0×10^{-7} eV per atom. *k*-point meshes of 8×8×8 Monkhorst-Pack schemes were used.

III. Results and discussion

The phase composition and crystallinity of the WO_3 sample prepared through a hydrogen peroxide-assisted route was evaluated by XRD analysis. The as-prepared

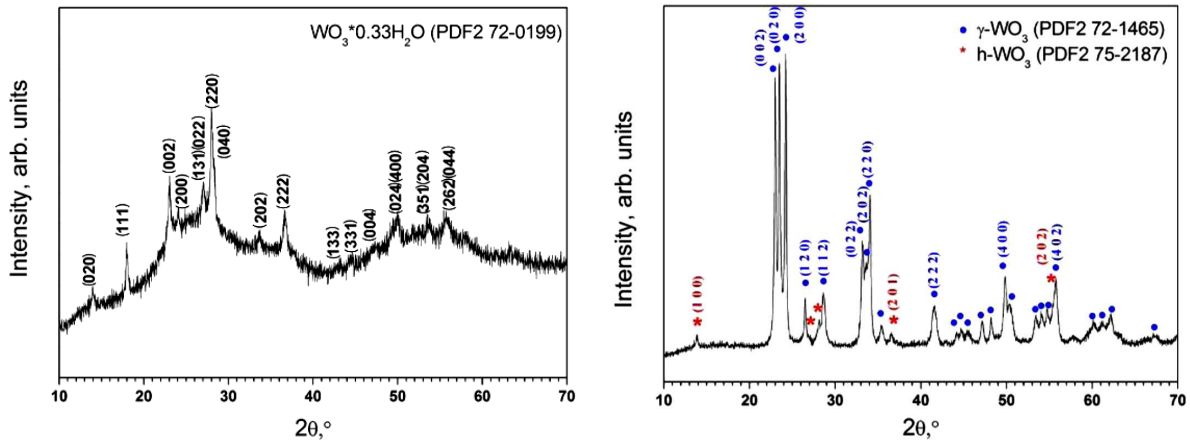

Figure 1. X-ray diffraction patterns of as-prepared sample of tungsten oxide (a) and the sample annealed at 400 °C (b)

product (Fig. 1a) contained both amorphous phase and crystalline hydrous tungsten oxide $WO_3 \cdot 0.33H_2O$ (PDF2 no. 72-0199), having an average particle size of 25 nm, as calculated using the Scherrer's formula. The dissolution mechanism of metallic tungsten in hydrogen peroxide for the synthesis of WO_3-based materials has been extensively discussed earlier [66–68]. Surprisingly, only very few attempts have been made to analyse the solid-state products formed upon ageing of peroxotungstic acid solutions. Wang *et al.* [67] showed that dissolution of metallic tungsten in H_2O_2 followed by ageing of the resultant sol at 55 °C yielded crystalline $WO_3 \cdot 2\,H_2O$. Enferadi-Kerenkan *et al.* [68] mentioned the formation of amorphous tungsten oxide upon rapid evaporation of a peroxotungstic acid solution, and the formation of crystalline $WO_2(O_2) \cdot H_2O$ upon its slow evaporation. Amorphous tungsten(VI)-oxide can be decomposed upon heating at relatively low temperatures (120 °C, 4 h), yielding $WO_3 \cdot 0.33H_2O$ and/or $WO_3 \cdot H_2O$ [68]. Thus, the phase composition of our as-prepared product, obtained through the hydrogen peroxide-assisted route, is in line with previously reported data, and corresponds to a mixture of amorphous tungsten oxide (obviously in hydrated form) and $WO_3 \cdot 0.33H_2O$.

According to scanning (Fig. 2a) and transmission (Fig. 3a) electron microscopy data, the as-obtained sample was a glassy monolith with the inclusion of flower-like crystals. The average size of these inclusions was 0.7–1.5 μm. Apparently, such flower-like morphology is typical of hydrous tungsten oxide $WO_3 \cdot 0.33H_2O$ [69].

The as-prepared semi-crystalline sample was further annealed at 400 °C for 2 h. Upon thermal treatment, a complete dehydration and crystallization occurred, and the resultant powder was found to consist of two WO_3 polymorphs (Fig. 1b), hexagonal (*h*-WO_3, sp. gr. *P*6/*mmm*, PDF2 no. 75-2187) and monoclinic (γ-WO_3, sp. gr. $P2_1/n$, PDF2 no. 72-1465). The average crystallite size, as calculated from X-ray line broadening by the Scherrer's method, amounted to 34 nm for the hexagonal WO_3 phase and 54 nm for the monoclinic WO_3 phase.

According to scanning and transmission electron microscopy, annealing at 400 °C led to complete crystallization of the powder. The annealed sample consisted of particles with a size of 40–55 nm merged into shapeless agglomerates (Figs. 2b and 3b). All the particles seemed to be uniform in shape and size and did not have any explicit faceting. The electron diffraction data are in a good agreement with XRD results. Low nitrogen adsorption measurements indicated that the annealing of the initial semi-amorphous sample resulted in a fivefold

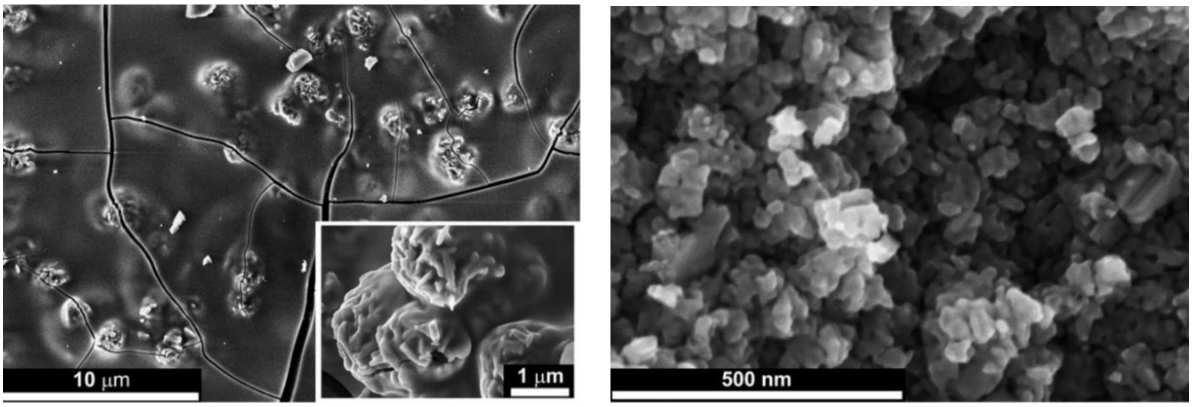

Figure 2. Scanning electron microscopy (SEM) images of: a) the as-prepared sample of hydrated tungsten oxide and b) the sample annealed at 400 °C (γ-WO_3/*h*-WO_3)

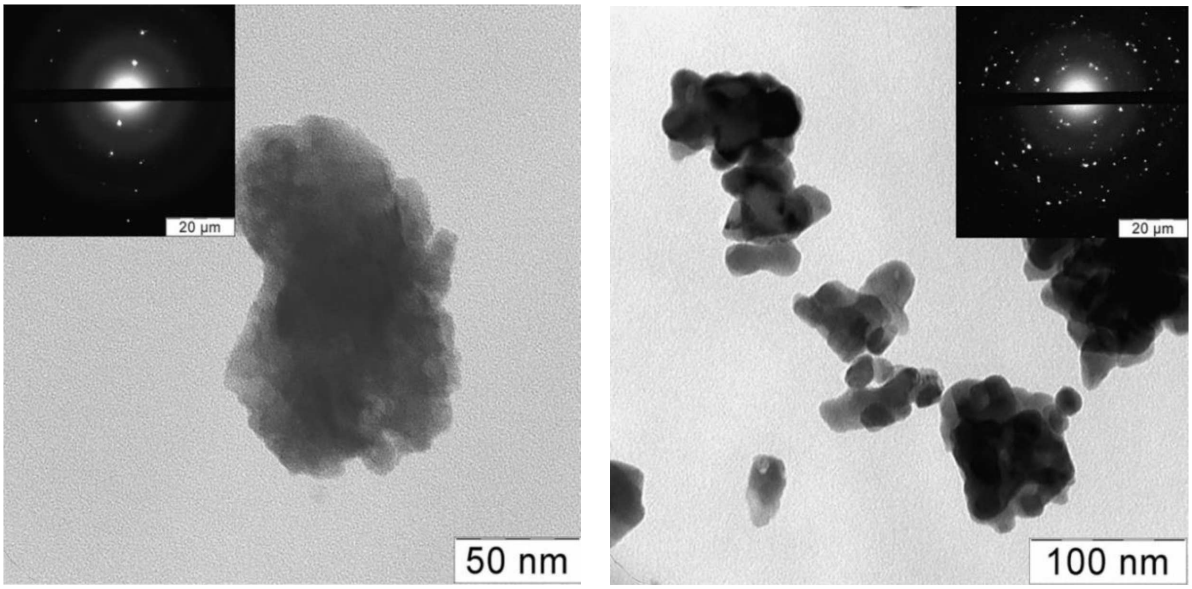

Figure 3. Transmission electron microscopy images and electron diffraction patterns of: a) the as-prepared sample of hydrated tungsten oxide and b) the sample annealed at 400 °C (γ-WO_3/h-WO_3)

increase in the specific surface area of the material, from 3 to 15 m^2/g.

Tungsten oxide with almost the same phase composition (h-WO_3/γ-WO_3) was obtained by thermal decomposition of ammonium paratungstate $(NH_4)_{10}H_2W_{12}O_{42} \cdot xH_2O$ at temperatures above 800 °C [70]. Until now, the factors governing the formation of various WO_3 polymorphs and their stabilization at ambient conditions have been poorly understood. It is well established that monoclinic WO_3 (γ-WO_3) is thermodynamically stable at room temperature, and that orthorhombic WO_3 (β-WO_3) is stable in the temperature range of 320–720 °C, while at higher temperatures tetragonal α-WO_3 is stable [71,72]. Comprehensive reports on various WO_3 polymorphs and their phase transitions have been presented previously [71,73]. High-temperature WO_3 phases can be stabilized for various reasons, e.g. due to the size effect [74]. Among WO_3 polymorphs, hexagonal WO_3 belongs to tungsten oxide bronzes, being a non-stoichiometric phase which always contains various impurities (e.g. NH_4^+, Na^+) located in the channels of its crystal structure [75]. In a hexagonal WO_3 structure, W^{6+}, W^{5+} and even W^{4+} ions are also present [75]. As the residual ions in the hexagonal channels are vital for stabilizing h-WO_3, its synthesis always involves the use of various tungstates. For example, hexagonal WO_3 phase can be synthesized via thermolysis of ammonium paratungstate [70,75], thermolysis or hydrothermal treatment of tungstic acid precipitated from sodium tungstate [76,77], etc. Upon the complete elimination of impurities from the structure of h-WO_3, its hexagonal framework collapses in an exothermic reaction, to form monoclinic WO_3 [75].

In our synthesis, we used only metallic tungsten, water and hydrogen peroxide, thus no cationic impurities such as NH_4^+ or Na^+ could stabilize the h-WO_3 structure. The possibility of pure h-WO_3 synthesis through a similar peroxide-assisted route was very recently reported by Tsuyumoto [78]; the formation of h-WO_3 required the presence of amorphized metal surfaces in the starting W powder, being a topochemical oxidation. Probably, the stability of h-WO_3 phase is also encouraged by the presence of water molecules and/or hydroxonium cations in the oxide network. A possible route for the formation of h-WO_3 could be the topochemical dehydration of hexagonal $WO_3 \cdot 0.33H_2O$, which has very similar diffraction pattern.

Tungsten oxides possess valuable electronic properties with possible applications as efficient photocatalysts and sensor materials. The electronic properties of various tungsten oxide-based semiconducting materials have been extensively discussed in the literature (see e.g. [49,62–65,79]). In this study, band structure and density of states (DOS) calculations were performed on two WO_3 polymorphs using hybrid (B3LYP and HSE) functionals. Previous experimental investigations of γ-WO_3 have found an indirect band gap ranging from 2.6 to 3.2 eV [80–82], while theoretical studies have shown that the band gap obtained with hybrid functionals is the closest to the experiment. In addition, theoreticians have pointed out that the energy difference between direct, Γ to Γ point, and indirect, Z to Γ point, band gaps is very small, giving the possibility for a direct band gap in γ-WO_3 phase [62–65]. DOS and band structure calculations for γ-WO_3 modification are presented in Fig. 4, showing an indirect band gap size of 2.45 eV, as calculated using B3LYP. Furthermore, special k-point directions in the Brillouin zone of the space group $P2_1/n$ (see Supporting Information) have been investigated, showing an in-line band in the Γ → Z direction. In addition, we can observe from the DOS that the valence bands (VB) are dominated by oxygen, and the conduction bands (CB) by tungsten, which is in good agree-

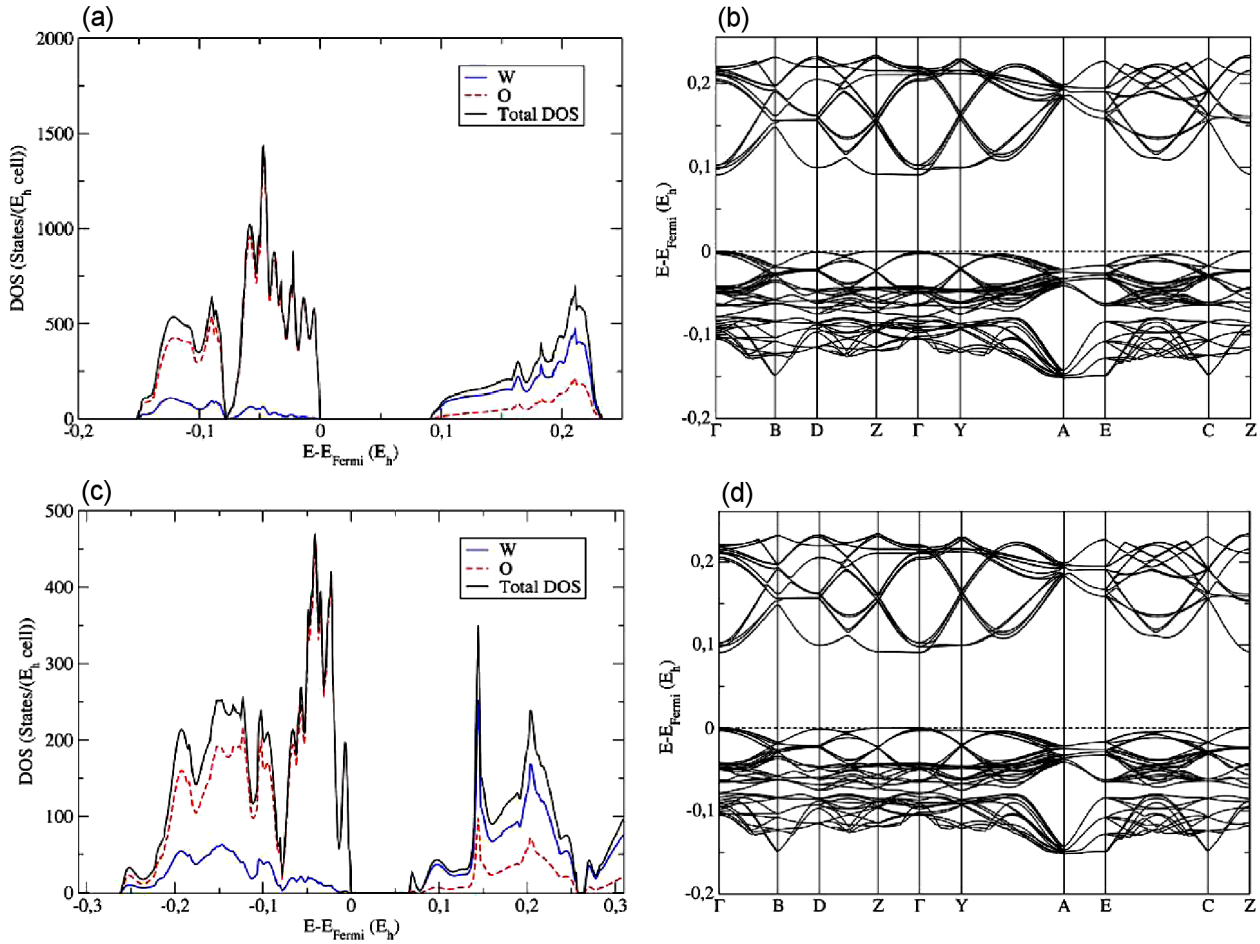

Figure 4. DOS (a) and band structure (b) of the γ-WO_3 modification; DOS (c) and band structure (d) of the *h*-WO_3 modification (calculation performed using the B3LYP functional)

ment with previous theoretical and experimental work [62–65,83].

The *h*-WO_3 modification has recently demonstrated possible optical and photoanode applications [49,84], although it has been much less investigated than the room temperature (RT) γ-WO_3 phase, especially concerning its electronic properties [85,86]. Figures 4c and 4d represent DOS and band structure calculations for *h*-WO_3 modification, respectively, clearly showing an indirect band gap of 1.79 eV, in agreement with previous theoretical work [85,86], since no direct measurements have yet been performed (see Supporting Information). In order to further investigate the electronic properties of hexagonal phase, special *k*-point directions in the Brillouin zone for the space group *P*6/*mmm* were chosen. We notice that the bottom of the CB is located at the Γ point and in-line with the M point, similar to the Γ → Z direction of the γ-WO_3 phase. The top of the VB is located at the A point, differently from the γ-WO_3 structure. However, the A point is in-line with the L point, showing the in-line band character of CB and VB, similar to the RT monoclinic phase. The DOS plots show that the VB are dominated by oxygen, and the CB by tungsten, again similar to the RT γ-WO_3 structure, which is in good agreement with previous theoretical work [85,86]. This shows the great diversity of electronic properties and complex structure-property relationships of *h*-WO_3 and γ-WO_3 modifications.

The design of composite materials comprising tungsten oxide has recently attracted special attention due to the possibility of tuning the electronic structure at the interface between two different semiconducting particles. Composites with a phase junction between *h*-WO_3 and monoclinic γ-WO_3 were recently reported to be highly efficient photocatalysts for the discolouration of organic dyes [70]. Note that the electronic structure of *h*-WO_3 is advantageous for water splitting applications of this material [49]. The difference in electronic band structure of γ-WO_3 and *h*-WO_3 was reported to facilitate the electron transfer through the junction surfaces and restrain the recombination of the charge carriers. Energy band diagrams at the γ-WO_3/*h*-WO_3 interface were reported very recently, indicating that such a phase junction facilitates redox reactions on the surface of a such phase-conjunct material [70,87]. Interestingly, other tungsten oxide-based composites possess a similar band gap structure at the phase junction interface. Recently, high photocatalytic activity due to the phase-junction effect was reported for the composite containing orthorhombic $WO_3 \cdot 0.33H_2O$ and *h*-WO_3 [88].

Extensive information is available on the synthesis of composite gas sensor materials containing semiconductors with different electronic properties (see e.g. a review paper by Miller *et al.* [46]). It has been established that the phase junction plays a key role in enhancing the sensor response of such materials. Since tungsten oxide is an *n*-type semiconductor with a band gap from 2.6 to 3.2 eV [80–82], the composites containing various WO_3 polymorphs belong to an *n-n* family of sensor materials [46]. In view of sensoric performance, a very important difference between *n-n* and *p-n* junctions is that the latter promote electron-hole recombination resulting in an increased interface resistance [89], while the former only transfer electrons from the oxide having the higher-energy conducting band into the oxide with the lower-energy band, forming an electron-rich layer. Recently, Sen *et al.* [90] reported superior sensor properties of an *n-n* composite comprising a $SnO_2/W_{18}O_{49}$ heterojunction.

Figure 5 shows the change in the resistance of the annealed WO_3 sample (γ-WO_3/*h*-WO_3) under the conditions of a cyclic change of the gas phase composition "air – 1 ppm NO_2 in air" with a stepwise decrease in the measured temperature from 300 to 25 °C. For each temperature, three measurement cycles were performed. In the presence of NO_2, the sample resistance increased due to the process:

$$NO_{2(gas)} + e^- \longleftrightarrow NO^-_{2(ads)} \quad (1)$$

accompanied by a decrease in the main charge carriers' concentration in an *n*-type semiconductor. The temperature dependence of the sensor response S, calculated as $S = R_{gas}/R_{air}$ (where R_{gas} is the sample resistance in the presence of NO_2, R_{air} is the resistance in pure air), is presented in the inset of Fig. 5. The maximum sensor response was observed at a measurement temperature of 100 °C. A very special feature of the material is a highly reproducible signal at room temperature (25 °C), which is better than that of any similar data presented elsewhere (Table 1).

Figure 6 demonstrates the change in the resistance of the WO_3 sample (γ-WO_3/*h*-WO_3) with a stepwise increase in the concentration of NO_2 in the air (0.1 – 0.2 – 0.5 – 1.0 ppm) at 100 °C. For each concentration, three measurement cycles were performed. Dependence of the sensor response on NO_2 concentration in double logarithmic coordinates demonstrated an almost linear behaviour, in accordance with power law theory [91].

Similar measurements performed at room temperature showed the absence of a sensor response for NO_2 concentrations of 0.1 and 0.2 ppm. In the presence of 0.5 ppm NO_2, an increase in WO_3 resistance was observed, while the signal increased very slowly. An increase in the concentration of NO_2 up to 2 ppm led to a growth in the resistance of the sensitive layer to more than $5 \cdot 10^{11}$ Ω, which was the upper limit of our measuring setup. The combination of these factors prevented the full calibration curve from being obtained at room temperature.

The comparison of the sensor response values for biphasic WO_3 (γ-WO_3/*h*-WO_3) synthesized by hydrogen peroxide assisted route with the literature data is shown in Fig. 7. It is necessary to take into account that the measurement methods varied in the different literature sources, which inevitably affects the calculated response values. In any case, the sensor response values obtained in this work are among the highest registered to date, even without any specific optimization of synthetic conditions, and despite the relatively low specific surface area of our WO_3 powder.

The literature survey showed that almost all results summarized in Fig. 7 were obtained using single-phased WO_3 sensor materials (mainly *h*-WO_3, γ-WO_3 and $W_{18}O_{49}$). However, in some cases, sensitive material comprised two different WO_3 phases, namely *h*-WO_3/γ-WO_3 [22,108] or β-WO_3/γ-WO_3 [104], and the authors

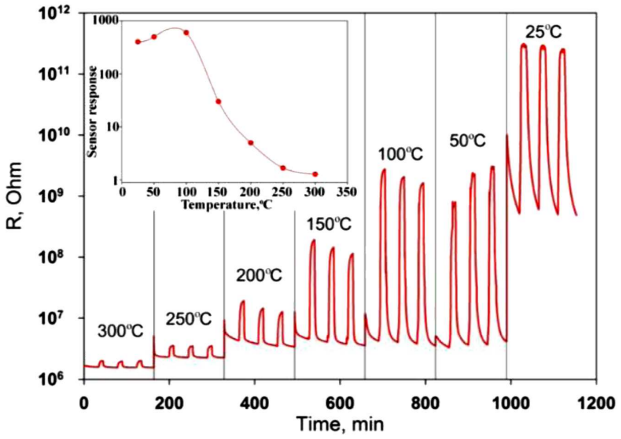

Figure 5. Resistance of WO_3 sample (γ-WO_3/*h*-WO_3) in the temperature range 300–25 °C under the periodic change of the gas phase composition (inset: Temperature dependence of the sensor response to 1 ppm NO_2 in the air)

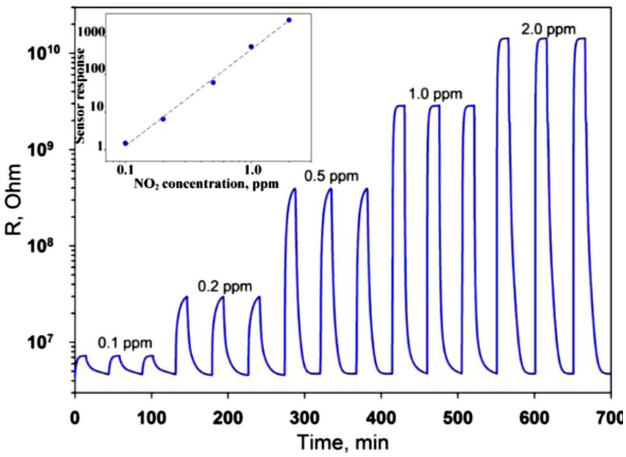

Figure 6. Resistance of WO_3 sample (γ-WO_3/*h*-WO_3) at 100 °C under the periodic change of NO_2 concentration in the air. Inset: Dependence of the sensor response at 100 °C on NO_2 concentration in the air (using double logarithmic coordinates)

Table 1. Response of WO_3-based sensors to NO_2 gas at room temperature

	Synthesis method	Sensor response $S = R_{NO_2}/R_{air}$	NO_2 concentration [ppm]	Ref.
WO_3/MWCNT* nanocomposite films	Decomposition of a metal organic compound	4.2	1	[117]
WO_3 nanoparticles/ porous Si	Sol-gel synthesis followed by dip-coating	2.0	1	[118]
WO_3/RGO** hybrids	CTAB*** assisted chemical precipitation	1.1	1	[119]
WO_3/RGO hybrids	Decomposition of a metal organic compound	1.8	1	[120]
WO_3 nanorods/porous Si	Hydrothermal synthesis	3.5	1	[121]
WO_3 nanoparticles (γ-WO_3/h-WO_3)	Peroxide route	450	1	This paper

*MWCNT – multi-walled carbon nanotube
**RGO – reduced graphene oxide
***CTAB – cetrimonium bromide; cetyltrimethylammonium bromide

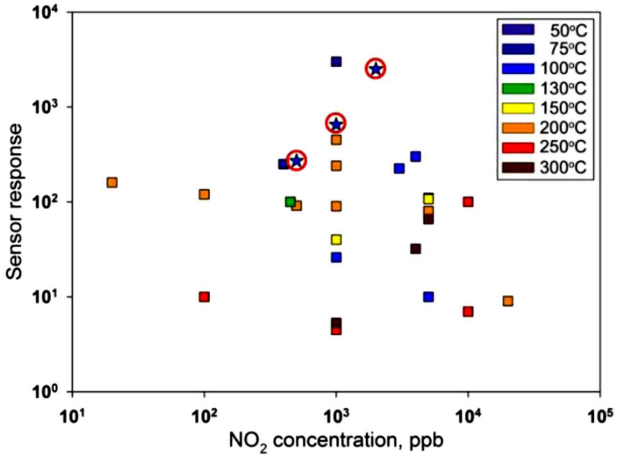

Figure 7. Comparison of the values of the sensor response of the WO_3 sample (γ-WO_3/h-WO_3) synthesized by peroxide-assisted route (circled asterisks) with the literature data [20,24,30,31,92–113] (squares) – the colour of the symbols corresponds to the measurement temperature

compared the response of these materials with single-phased WO_3 synthesized using a similar approach. In all cases, the sensitivity of the composite materials appeared to be higher than that of the single-phased materials, but this feature has not been discussed at all. Similarly, biphase material has shown the best sensor response towards NO_2 than other gases, which together with effect of humidity should be investigated in greater detail in future studies.

As follows from Fig. 1b, the main phase in the material synthesized in this work is γ-WO_3, the content of h-WO_3 being about 5–10 wt.%. Hexagonal h-WO_3 has a higher energy conduction band than monoclinic γ-WO_3 [114,115]. Thus, in the junction zone of these two phases, electron transfer from h-WO_3 to γ-WO_3 occurs. As a result, the concentration of charge carriers increases in the γ-WO_3 phase, which provides the main conduction path through the material. In our previous studies of gallium doped zinc oxide [116], it has been shown that an increase in electron concentration leads to an increase in the sensor response of n-type semiconductor oxide in the detection of NO_2, (this gas is an electron acceptor), due to the shift of equilibrium in Eq. 1 to the right. So, it is reasonable to assume that it is an increase in the concentration of electrons in the γ-WO_3 phase (due to their transfer from h-WO_3) that is the cause of the enhanced sensor response of the obtained WO_3/WO_3-composite material. Furthermore, we hope that this study will open new fields of investigations (e.g. XPS since the valence state of tungsten was so important in the synthesis and properties) in order to take a look into this mix-phase material, ratio and stability of the phases, and to further investigate and understand the mechanism of the NO_2 sensing.

IV. Conclusions

In this work highly crystalline tungsten oxide was synthesized via a facile low-temperature peroxide-mediated route. Afterwards, the synthesized material was experimentally and theoretically characterized and electrical properties investigated using *ab initio* calculations and *in situ* measurements. The synthesized material is the h-WO_3/γ-WO_3 composite, which showed excellent sensor response towards NO_2 and had the highest reported level. Room temperature sensor response exceeded recently reported data by more than two orders of magnitude. The possible reason for the enhanced sensor response of the composite is an electron transfer from h-WO_3 to γ-WO_3 phase.

Acknowledgements: Authors Olga S. Ivanova, Alexander E. Baranchikov, Taisiya O. Shekunova, Khursand E. Yorov, Olga M. Gajtko, Lili Yang, Marina N. Rumyantseva and Vladimir K. Ivanov received funding from by the Russian Science Foundation (project 18-73-10150). Authors Branko Matović, Jelena Luković and Dejan

Zagorac received funding from the Ministry of Education, Science and Technological Development of the Republic of Serbia, Grant 45012.

§ Supporting Information can be downloaded using following link: https://bit.ly/3qhTy90

References

1. K. Thummavichai, Y. Xia, Y. Zhu, "Recent progress in chromogenic research of tungsten oxides towards energy-related applications", *Prog. Mater. Sci.*, **88** (2017) 281–324.
2. A. Gheno, T.T. Thu Pham, C.Di Bin, J. Bouclé, B. Ratier, S. Vedraine, "Printable WO_3 electron transporting layer for perovskite solar cells: Influence on device performance and stability", *Sol. Energy Mater. Sol. Cells*, **161** (2017) 347–354.
3. P.A. Shinde, A.C. Lokhande, A.M. Patil, C.D. Lokhande, "Facile synthesis of self-assembled WO_3 nanorods for high-performance electrochemical capacitor", *J. Alloys Compd.*, **770** (2019) 1130–1137.
4. A.L. Popov, O.B. Balko, A.E. Baranchikov, N.M. Zholobak, O.S. Ivanova, V.K. Ivanov, A.B. Shcherbakov, O.I. Balko, N.R. Popova, "Photo-induced toxicity of tungsten oxide photochromic nanoparticles", *J. Photochem. Photobiol. B Biol.*, **178** (2017) 395–403.
5. V.R. Buch, A.K. Chawla, S.K. Rawal, "Review on electrochromic property for WO_3 thin films using different deposition techniques", *Mater. Today Proc.*, **3** [6] (2016) 1429–1437.
6. M. Parthibavarman, M. Karthik, S. Prabhakaran, "Facile and one step synthesis of WO_3 nanorods and nanosheets as an efficient photocatalyst and humidity sensing material", *Vacuum*, **155** (2018) 224–232.
7. B.S. Kalanoor, H. Seo, S.S. Kalanur, "Recent developments in photoelectrochemical water-splitting using WO_3/$BiVO_4$ heterojunction photoanode: A review", *Mater. Sci. Energy Technol.*, **1** [1] (2018) 49–62.
8. J. Huang, X. Xu, C. Gu, G. Fu, W. Wang, J. Liu, "Flower-like and hollow sphere-like WO_3 porous nanostructures: Selective synthesis and their photocatalysis property", *Mater. Res. Bull.*, **47** [11] (2012) 3224–3232.
9. S. Zhang, H. Li, Z. Yang, "Controllable synthesis of WO_3 with different crystalline phases and its applications on methylene blue removal from aqueous solution", *J. Alloys Compd.*, **722** (2017) 555–563.
10. S. Yao, F. Qu, G. Wang, X. Wu, "Facile hydrothermal synthesis of WO_3 nanorods for photocatalysts and supercapacitors", *J. Alloys Compd.*, **724** (2017) 695–702.
11. Y. Shen, H. Bi, T. Li, X. Zhong, X. Chen, A. Fan, D. Wei, "Low-temperature and highly enhanced NO_2 sensing performance of Au-functionalized WO_3 microspheres with a hierarchical nanostructure", *Appl. Surf. Sci.*, **434** (2018) 922–931.
12. M. Ye, G. Chen, X. Chu, C. Gao, C.-Y. Guo, H. Qiao, J. Chen, "Thickness controllable single-crystal WO_3 nanosheets: Highly selective sensor for triethylamine detection at room temperature", *Mater. Lett.*, **226** (2018) 59–62.
13. Y. Yanyan, L. Chen, X. Jingkun, D. Wei, S. Chengwen, "Synthesis, characterization, and gas sensing properties of WO_3 nanoplates", *Rare Met. Mater. Eng.*, **46** [5] (2017) 1241–1244.
14. Y. Yuan, H. Yang, M. Wang, L. Wang, B. Liu, J. Yang, Q. Du, H. Zhao, Y. Ren, X. Zhang, J. Liu, "Enhancing gas sensing performances and sensing mechanism at atomic and molecule level of WO_3 nanoparticles by hydrogenation", *Sensor. Actuat. B Chem.*, **273** (2018) 1786–1793.
15. A. Fioravanti, S. Morandi, M.C. Carotta, "Chemoresistive gas sensors for sub-ppm acetone detection", *Procedia Eng.*, **168** (2016) 485–488.
16. M.B. Rahmani, M.H. Yaacob, Y.M. Sabri, "Hydrogen sensors based on 2D WO_3 nanosheets prepared by anodization", *Sensor. Actuat. B Chem.*, **251** (2017) 57–64.
17. H.M. Lin, C.M. Hsu, H.Y. Yang, P.Y. Lee, C.C. Yang, "Nanocrystalline WO_3-based H_2S sensors", *Sensor. Actuat. B. Chem.*, **22** [1] (1994) 63–68.
18. A.E. Shekunova, T.O. Baranchikov, A.D. Yapryntsev, P.G. Rudakovskaya, O.S. Ivanova, Y.A. Karavanova, M.A. Kalinina, M.N. Rumyantseva, S.G. Dorofeev, V.K. Ivanov, "Ultrasonic disintegration of tungsten trioxide pseudomorphs after ammonium paratungstate as a route for stable aqueous sols of nanocrystalline WO_3", *J. Mater. Sci.*, **53** [3] (2018) 1758–1768.
19. Z.X. Cai, H.Y. Li, J.C. Ding, X. Guo, "Hierarchical flower-like WO_3 nanostructures assembled by porous nanoflakes for enhanced NO gas sensing", *Sensor. Actuat. B Chem.*, **246** (2017) 225–234.
20. D. Meng, T. Yamazaki, Y. Shen, Z. Liu, T. Kikuta, "Preparation of WO_3 nanoparticles and application to NO_2 sensor", *Appl. Surf. Sci.*, **256** [4] (2009) 1050–1053.
21. V.V. Ganbavle, S.V. Mohite, J.H. Kim, K.Y. Rajpure, "Effect of solution concentration on physicochemical and gas sensing properties of sprayed WO_3 thin films", *Curr. Appl. Phys.*, **15** [2] (2015) 84–93.
22. C. Wang, M. Ding, X. Kou, L. Guo, C. Feng, X. Li, H. Zhang, P. Sun, Y. Sun, G. Lu, "Detection of nitrogen dioxide down to ppb levels using flower-like tungsten oxide nanostructures under different annealing temperatures", *J. Colloid Interf. Sci.*, **483** [2] (2016) 314–320.
23. Z. Wang, D. Wang, J. Sun, "Controlled synthesis of defect-rich ultrathin two-dimensional WO_3 nanosheets for NO_2 gas detection", *Sensor. Actuat. B Chem.*, **245** (2017) 828–834.
24. Z. Wang, M. Hu, Y. Qin, "Solvothermal synthesis of WO_3 nanocrystals with nanosheet and nanorod morphologies and the gas-sensing properties", *Mater. Lett.*, **171** [43] (2016) 146–149.
25. Z. Wang, M. Hu, Y. Wang, X. Liu, Y. Qin, "Effect of solvothermal reaction temperature on the morphology of WO_3 nanocrystals and their low-temperature NO_2-sensing properties", *J. Alloys Compd.*, **665** (2016) 173–179.
26. K. Khojier, H. Savaloni, N. Habashi, M.H. Sadi, "On the influence of temperature gradient of annealing process on the nano-structure and sensing properties of WO_3 thin films to NO_2 gas and relative humidity", *Mater. Sci. Semicond. Process.*, **41** [2] (2016) 177–183.
27. L. Giancaterini, S.M. Emamjomeh, A.De Marcellis, E. Palange, A. Resmini, U. Anselmi-Tamburini, C. Cantalini, "The influence of thermal and visible light activation modes on the NO_2 response of WO_3 nanofibers prepared by electrospinning", *Sensor. Actuat. B Chem.*, **229** [2] (2016) 387–395.
28. S. Cao, H. Chen, "Nanorods assembled hierarchical urchin-like WO_3 nanostructures: Hydrothermal synthesis, characterization, and their gas sensing properties", *J. Alloys Compd.*, **702** (2017) 644–648.

29. S. Cao, Y. Zhang, Y. Liu, J. Chen, L. Zhang, L. Han, "Facile synthesis of hierarchical carpet-like WO_3 microflowers for high NO_2 gas sensing performance", *Mater. Lett.*, **210** (2017) 8–11.
30. V.L. Patil, J.L. Bhosale, S.S. Shendage, S.A. Vanalakar, S.P. Patil, P.S. Patil, J.H. Kim, N.S. Harale, "Sensitive and selective NO_2 gas sensor based on WO_3 nanoplates", *Sensor. Actuat. B Chem.*, **240** [2] (2016) 426–433.
31. Y. Sun, F. Liu, C. Wang, R. Sun, G. Lu, P. Sun, X. Li, "Hierarchical flower-like WO_3 nanostructures and their gas sensing properties", *Sensor. Actuat. B Chem.*, **204** (2014) 224–230.
32. D. Li, J. Sun, R. Luo, A. Chen, S. Bai, B. Song, K. Zhang, J. Ye, J. Guo, "Synthesis of Sb doping hierarchical WO_3 microspheres and mechanism of enhancing sensing properties to NO_2", *J. Alloys Compd.*, **692** [2] (2016) 876–884.
33. B. Xiao, D. Wang, F. Wang, Q. Zhao, C. Zhai, M. Zhang, "Preparation of hierarchical WO_3 dendrites and their applications in NO_2 sensing", *Ceram. Int.*, **43** [11] (2017) 8183–8189.
34. A. Maity, S.B. Majumder, "NO_2 sensing and selectivity characteristics of tungsten oxide thin films", *Sensor. Actuat. B Chem.*, **206** [2] (2015) 423–429.
35. A.T. Mane, S.B. Kulkarni, S.T. Navale, A.A. Ghanwat, N.M. Shinde, J. Kim, V.B. Patil, "NO_2 sensing properties of nanostructured tungsten oxide thin films", *Ceram. Int.*, **40** [10] (2014) 16495–16502.
36. M. Takács, A.E. Pap, "Gas sensitivity of sol-gel prepared mesoporous WO_3 thin film", *Procedia Eng.*, **168** (2016) 289–292.
37. Y. Chai, F.Y. Ha, F.K. Yam, Z. Hassan, "Fabrication of tungsten oxide nanostructure by sol-gel method", *Procedia Chem.*, **19** (2016) 113–118.
38. S.S. Shendage, V.L. Patil, S.P. Patil, S.A. Vanalakar, J.L. Bhosale, J.H. Kim, P.S. Patil, "NO_2 sensing properties of porous fibrous reticulated WO_3 thin films", *J. Anal. Appl. Pyrolysis*, **125** [2] (2017) 9–16.
39. J.H. Kim, K.Y. Rajpure, S.V. Mohite, G.L. Agawane, V.V. Ganbavle, "Nitrogen dioxide sensing properties of sprayed tungsten oxide thin film sensor: Effect of film thickness", *J. Colloid Interf. Sci.*, **451** [2] (2015) 245–254.
40. C. Wang, X. Li, C. Feng, Y. Sun, G. Lu, "Nanosheets assembled hierarchical flower-like WO_3 nanostructures: Synthesis, characterization, and their gas sensing properties", *Sensor. Actuat. B Chem.*, **210** (2015) 75–81.
41. T. Kida, A. Nishiyama, M. Yuasa, K. Shimanoe, N. Yamazoe, "Highly sensitive NO_2 sensors using lamellar-structured WO_3 particles prepared by an acidification method", *Sensor. Actuat. B Chem.*, **135** [2] (2009) 568–574.
42. S. Kabcum, N. Kotchasak, D. Channei, A. Tuantranont, A. Wisitsoraat, S. Phanichphant, C. Liewhiran, "Highly sensitive and selective NO_2 sensor based on Au-impregnated WO_3 nanorods", *Sensor. Actuat. B Chem.*, **252** [2] (2017) 523–536.
43. B. Behera, S. Chandra, "Synthesis of WO_3 nanorods by thermal oxidation technique for NO_2 gas sensing application", *Mater. Sci. Semicond. Process.*, **86** [2] (2018) 79–84.
44. J. Sungpanich, T. Thongtem, S. Thongtem, "Fabrication of WO_3 nanofibers by high voltage electrospinning", *Mater. Lett.*, **65** [19-20] (2011) 3000–3004.
45. S. Nazarpour, E. Marzbanrad, E.K. Heidari, C. Zamani, B. Raissi, "WO_3-based NO_2 sensors fabricated through low frequency AC electrophoretic deposition", *Sensor. Actuat B Chem.*, **146** [1] (2010) 165–170.
46. D.R. Miller, S.A. Akbar, P.A. Morris, "Nanoscale metal oxide-based heterojunctions for gas sensing: A review", *Sensor. Actuat. B Chem.*, **204** (2014) 250–272.
47. A. Szczygielska, Z. Pedzich, W. Maziarz, "Nanocrystalline composites in TiO_2 and SnO_2 system for ammonia resistance sensors", *Process. Appl. Ceram.*, **12** [3] (2018) 240–247.
48. J.C. Alvarez-Quiceno, G. Dalpian, J.M. Osorio-Guillén, "A systematic first-principles study of the tungsten trioxide polymorphs", *Phys. Status Solidi*, **252** [10] (2015) 2290–2295.
49. T. Lee, Y. Lee, W. Jang, A. Soon, "Understanding the advantage of hexagonal WO_3 as an efficient photoanode for solar water splitting: A first-principles perspective", *J. Mater. Chem. A*, **4** [29] (2016) 11498–11506.
50. D. Nagy, D. Nagy, I. M. Szilágyi, X. Fan, "Effect of the morphology and phases of WO_3 nanocrystals on their photocatalytic efficiency", *RSC Adv.*, **6** [40] (2016) 33743–33754.
51. N.R. Elezović, B.M. Babić, L. Gajić-Krstajić, P. Ercius, V.R. Radmilović, N.V. Krstajić, L.M. Vračar, "Pt supported on nano-tungsten carbide as a beneficial catalyst for the oxygen reduction reaction in alkaline solution", *Electrochim. Acta*, **69** (2012) 239–246.
52. M. Hepel, S. Hazelton, "Photoelectrocatalytic degradation of diazo dyes on nanostructured WO_3 electrodes", *Electrochim. Acta*, **50** [25-26] (2005) 5278–5291.
53. T. Siegrist, "Crystallographica - A software toolkit for crystallography", *J. Appl. Crystallogr.*, **30** [3] (2002) 418–419.
54. R. Dovesi, A. Erba, R. Orlando, C. M. Zicovich-Wilson, B. Civalleri, L. Maschio, M. Rérat, S. Casassa, J. Baima, S. Salustro, B. Kirtman, "Quantum-mechanical condensed matter simulations with CRYSTAL", *Wiley Interdiscip. Rev. Comput. Mol. Sci.*, **8** [4] (2018) e1360.
55. J. Heyd, G.E. Scuseria, M. Ernzerhof, "Hybrid functionals based on a screened Coulomb potential", *J. Chem. Phys.*, **118** [18] (2003) 8207–8215.
56. A.D. Becke, "Density functional thermochemistry. III. The role of exact exchange", *J. Chem. Phys.*, **98** [7] (1993) 5648–5652.
57. M.D. Towler, N.L. Allan, N.M. Harrison, V.R. Saunders, W.C. Mackrodt, E. Aprà, "Ab initio study of MnO and NiO", *Phys. Rev. B*, **50** [8] (1994) 5041–5054.
58. D. Zagorac, J.C. Schön, J. Zagorac, M. Jansen, "Prediction of structure candidates for zinc oxide as a function of pressure and investigation of their electronic properties", *Phys. Rev. B*, **89** [7] (2014) 075201.
59. D. Zagorac, J. Zagorac, J.C. Schön, N. Stojanović, B. Matović, "ZnO/ZnS (hetero)structures: ab initio investigations of polytypic behavior of mixed ZnO and ZnS compounds", *Acta Crystallogr. B*, **74** [6] (2018) 628–642.
60. D. Andrae, U. Häußermann, M. Dolg, H. Stoll, H. Preuß, "Energy-adjustedab initio pseudopotentials for the second and third row transition elements", *Theor. Chim. Acta*, **77** [2] (1990) 123–141.
61. J. Luković, D. Zagorac, J.C. Schön, J. Zagorac, D. Jordanov, T. Volkov-Husović, B. Matović, "Tungsten disilicide (WSi_2): Synthesis, characterization, and prediction of new crystal structures", *Z. Anorg. Allg. Chemie*, **643** [23] (2017) 2088–2094.

62. H. Hamdi, E.K.H. Salje, P. Ghosez, E. Bousquet, "First-principles reinvestigation of bulk WO_3", *Phys. Rev. B*, **94** [24] (2016) 245124.
63. R. Chatten, A.V. Chadwick, A. Rougier, P.J.D. Lindan, "The oxygen vacancy in crystal phases of WO_3", *J. Phys. Chem. B*, **109** [8] (2005) 3146–3156.
64. Y. Ping, G. Galli, "Optimizing the band edges of tungsten trioxide for water oxidation: A first-principles study", *J. Phys. Chem. C*, **118** [12] (2014) 6019–6028.
65. F. Wang, C. Di Valentin, G. Pacchioni, "Electronic and structural properties of WO_3: A systematic hybrid DFT study", *J. Phys. Chem. C*, **115** [16] (2011) 8345–8353.
66. L. Zhou, J. Zou, M. Yu, P. Lu, J. Wei, Y. Qian, Y. Wang, C. Yu, "Green synthesis of hexagonal-shaped $WO_3 \cdot 0.33H_2O$ nanodiscs composed of nanosheets", *Cryst. Growth Des.*, **8** [11] (2008) 3993–3998.
67. J. Wang, P.S. Lee, J. Ma, "Synthesis, growth mechanism and room-temperature blue luminescence emission of uniform WO_3 nanosheets with W as starting material", *J. Cryst. Growth*, **311** [2] (2009) 316–319.
68. A. Enferadi-Kerenkan, A.S. Ello, T.O. Do, "Synthesis, organo-functionalization, and catalytic properties of tungsten oxide nanoparticles as heterogeneous catalyst for oxidative cleavage of oleic acid as a model fatty acid into diacids", *Ind. Eng. Chem. Res.*, **56** [38] (2017) 10639–10647.
69. Q.-H. Li, L.-M. Wang, D.-Q. Chu, X.-Z. Yang, Z.-Y. Zhang, "Cylindrical stacks and flower-like tungsten oxide microstructures: Controllable synthesis and photocatalytic properties", *Ceram. Int.*, **40** [3] (2014) 4969–4973.
70. Y. Lu, G. Liu, J. Zhang, Z. Feng, C. Li, Z. Li, "Fabrication of a monoclinic/hexagonal junction in WO_3 and its enhanced photocatalytic degradation of rhodamine B", *Chinese J. Catal.*, **37** [3] (2016) 349–358.
71. T. Vogt, P.M. Woodward, B.A. Hunter, "The high-temperature phases of WO_3", *J. Solid State Chem.*, **144** [1] (1999) 209–215.
72. E. Salje, "The orthorhombic phase of WO_3", *Acta Crystallogr. B*, **33** [2] (2002) 574–577.
73. H. Kalhori, M. Ranjbar, H. Salamati, J.M.D. Coey, "Flower-like nanostructures of WO_3: Fabrication and characterization of their in-liquid gasochromic effect", *Sensor. Actuat. B Chem.*, **225** (2016) 535–543.
74. M. Boulova, G. Lucazeau, "Crystallite nanosize effect on the structural transitions of WO_3 studied by Raman spectroscopy", *J. Solid State Chem.*, **167** [2] (2002) 425–434.
75. I.M. Szilágyi, J. Madarász, G. Pokol, P. Király, G. Tárkányi, S. Saukko, J. Mizsei, A.L. Tóth, A. Szabó, K. Varga-Josepovits, "Stability and controlled composition of hexagonal WO_3", *Chem. Mater.*, **20** [12] (2008) 4116–4125.
76. B. Gerand, G. Nowogrocki, J. Guenot, M. Figlarz, "Structural study of a new hexagonal form of tungsten trioxide", *J. Solid State Chem.*, **29** [3] (1979) 429–434.
77. J. Pfeifer, E.O. Zayim, A.L. Tóth, L. Wang, K. Sedlacková, I.M. Szilágyi, P.-I. Gouma, C. Balázsi, "Nanosize hexagonal tungsten oxide for gas sensing applications", *J. Eur. Ceram. Soc.*, **28** [5] (2007) 913–917.
78. I. Tsuyumoto, "Facile synthesis of nanocrystalline hexagonal tungsten trioxide from metallic tungsten powder and hydrogen peroxide", *J. Am. Ceram. Soc.*, **101** [2] (2018) 509–514.
79. A. Hjelm, C.G. Granqvist, J.M. Wills, "Electronic structure and optical properties of WO_3", *Phys. Rev. B*, **54** [4] (1996) 2436–2445.
80. C.G. Granqvist, *Handbook of Inorganic Electrochromic Materials*, Elsevier Science B.V., Amsterdam, 1995.
81. F.P. Koffyberg, K. Dwight, A. Wold, "Interband transitions of semiconducting oxides determined from photoelectrolysis spectra", *Solid State Commun.*, **30** [7] (1979) 433–437.
82. P.P. González-Borrero, F. Sato, A.N. Medina, M.L. Baesso, A.C. Bento, G. Baldissera, C. Persson, G.A. Niklasson, C.G. Granqvist, A. Ferreira da Silva, "Optical band-gap determination of nanostructured WO_3 film", *Appl. Phys. Lett.*, **96** [6] (2010) 061909.
83. H. Zheng, J.Z. Ou, M.S. Strano, R.B. Kaner, A. Mitchell, K. Kalantar-zadeh, R.B. Kaner, H. Zheng, J.Z. Ou, M.S. Strano, A. Mitchell, "Nanostructured tungsten oxide - Properties, synthesis, and applications", *Adv. Funct. Mater.*, **21** [12] (2011) 2175–2196.
84. Y. Lee, T. Lee, W. Jang, A. Soon, "Unraveling the intercalation chemistry of hexagonal tungsten bronze and its optical responses", *Chem. Mater.*, **28** [13] (2016) 4528–4535.
85. P. Krüger, I. Koutiri, S. Bourgeois, "First-principles study of hexagonal tungsten trioxide: Nature of lattice distortions and effect of potassium doping", *Phys. Rev. B*, **86** [22] (2012) 224102.
86. Y. Lee, T. Lee, A. Soon, "Polytypism in hexagonal tungsten trioxide: Insights from ab initio molecular dynamics simulations", *J. Phys. Chem. C*, **122** [37] (2018) 21644–21650.
87. Z. Feng, F. Wang, J. Zhang, X. Chen, C. Li, Y. Lu, "K_2SO_4-assisted hexagonal/monoclinic WO_3 phase junction for efficient photocatalytic degradation of RhB", *ACS Appl. Energy Mater.*, **1** [5] (2018) 2067–2077.
88. Y. Li, Z. Tang, J. Zhang, Z. Zhang, "Fabrication of vertical orthorhombic/hexagonal tungsten oxide phase junction with high photocatalytic performance", *Appl. Catal. B Environ.*, **207** (2017) 207–217.
89. I. Giebelhaus, E. Varechkina, T. Fischer, M. Rumyantseva, V. Ivanov, A. Gaskov, J.R. Morante, J. Arbiol, W. Tyrra, S. Mathur, "One-dimensional CuO-SnO_2 p-n heterojunctions for enhanced detection of H_2S", *J. Mater. Chem. A*, **1** [37] (2013) 11261–11268.
90. S. Sen, P. Kanitkar, A. Sharma, K.P. Muthe, A. Rath, S.K. Deshpande, M. Kaur, R.C. Aiyer, S.K. Gupta, J.V. Yakhmi, "Growth of $SnO_2/W_{18}O_{49}$ nanowire hierarchical heterostructure and their application as chemical sensor", *Sensor. Actuat. B Chem.*, **147** [2] (2010) 453–460.
91. N. Yamazoe, K. Shimanoe, "Theory of power laws for semiconductor gas sensors", *Sensor. Actuat. B Chem.*, **128** [2] (2008) 566–573.
92. N.M.A. Hadia, M.S. Alqahtani, S.H. Mohamed, "WO_3 nanowires for optoelectronic and gas sensing applications", *Appl. Phys. A*, **119** [4] (2015) 1261–1267.
93. L.G. Teoh, Y.M. Hon, J. Shieh, W.H. Lai, M.H. Hon, "Sensitivity properties of a novel NO_2 gas sensor based on mesoporous WO_3 thin film", *Sensor. Actuat. B Chem.*, **96** [1-2] (2003) 219–225.
94. C.S. Rout, K. Ganesh, A. Govindaraj, C.N.R. Rao, "Sensors for the nitrogen oxides, NO_2, NO and N_2O, based on In_2O_3 and WO_3 nanowires", *Appl. Phys. A*, **85** [3] (2006) 241–246.
95. J. Zeng, M. Hu, W. Wang, H. Chen, Y. Qin, "NO_2-sensing properties of porous WO_3 gas sensor based on anodized

sputtered tungsten thin film", *Sensor. Actuat. B Chem.*, **161** [1] (2012) 447–452.
96. D.S. Lee, K.H. Nam, D.D. Lee, "Effect of substrate on NO_2-sensing properties of WO_3 thin film gas sensors", *Thin Solid Films*, **375** [1-2] (2000) 142–146.
97. X. An, J.C. Yu, Y. Wang, Y. Hu, X. Yu, G. Zhang, "WO_3 nanorods/graphene nanocomposites for high-efficiency visible-light-driven photocatalysis and NO_2 gas sensing", *J. Mater. Chem.*, **22** [17] (2012) 8525–8531.
98. X. He, J. Li, X. Gao, L. Wang, "NO_2 sensing characteristics of WO_3 thin film microgas sensor", *Sensor. Actuat. B Chem.*, **93** [1-3] (2003) 463–467.
99. Y. Shen, T. Yamazaki, Z. Liu, D. Meng, T. Kikuta, N. Nakatani, "Influence of effective surface area on gas sensing properties of WO_3 sputtered thin films", *Thin Solid Films*, **517** [6] (2009) 2069–2072.
100. J. Tamaki, "Grain-size effects in tungsten oxide-based sensor for nitrogen oxides", *J. Electrochem. Soc.*, **141** [8] (2006) 2207–2210.
101. Y.G. Choi, G. Sakai, K. Shimanoe, N. Yamazoe, "Wet process-based fabrication of WO_3 thin film for NO_2 detection", *Sensor. Actuat. B Chem.*, **101** [1-2] (2004) 107–111.
102. A. Boudiba, C. Zhang, H. Liao, M. Debliquy, C. Coddet, "Sensing properties of atmospheric plasma-sprayed WO_3 coating for sub-ppm NO_2 detection", *Sensor. Actuat. B Chem.*, **144** [1] (2009) 280–288.
103. Y. Qin, M. Hu, J. Zhang, "Microstructure characterization and NO_2-sensing properties of tungsten oxide nanostructures", *Sensor. Actuat. B Chem.*, **150** [1] (2010) 339–345.
104. M. Carotta, M. Sacerdoti, V. Guidi, A. Giberti, M. Blo, C. Malagù, B. Vendemiati, S. Galliera, G. Martinelli, M. Butturi, M. Piga, "Aqueous and alcoholic syntheses of tungsten trioxide powders for NO_2 detection", *Sensor. Actuat. B Chem.*, **100** [1-2] (2004) 277–282.
105. N. Van Hieu, H. Van Vuong, N. Van Duy, N.D. Hoa, "A morphological control of tungsten oxide nanowires by thermal evaporation method for sub-ppm NO_2 gas sensor application", *Sensor. Actuat. B Chem.*, **171-172** (2012) 760–768.
106. Z. Hua, C. Tian, Z. Qiu, Y. Li, X. Tian, M. Wang, E. Li, "An investigation on NO_2 sensing mechanism and shielding behavior of WO_3 nanosheets", *Sensor. Actuat. B Chem.*, **259** (2018) 250–257.
107. Y. Shen, X. Chen, W. Wang, Y. Gong, S. Chen, J. Liu, D. Wei, D. Meng, X. San, "Complexing surfactants-mediated hydrothermal synthesis of WO_3 microspheres for gas sensing applications", *Mater. Lett.*, **163** (2016) 150–153.
108. L. You, X. He, D. Wang, P. Sun, Y.F. Sun, X.S. Liang, Y. Du, G.Y. Lu, "Ultrasensitive and low operating temperature NO_2 gas sensor using nanosheets assembled hierarchical WO_3 hollow microspheres", *Sensor. Actuat. B Chem.*, **173** (2012) 426–432.
109. J.-W. Yoon, Y.J. Hong, J.-H. Lee, Y.C. Kang, A.A. Wazzan, F. Abdel-Hady, J.-S. Kim, "Highly sensitive and selective detection of ppb-level NO_2 using multi-shelled WO_3 yolk-shell spheres", *Sensor. Actuat. B Chem.*, **229** (2016) 561–569.
110. T. Sanada, J. Tamaki, N. Wada, T. Suzuki, K. Kojima, Z. Meng, H. Haneoka, T. Hashishin, A. Fujii, "Morphological and crystal structural control of tungsten trioxide for highly sensitive NO_2 gas sensors", *J. Mater. Chem. C*, **3** [5] (2014) 1134–1141.
111. S. Bai, K. Zhang, R. Luo, D. Li, A. Chen, C.C. Liu, "Low-temperature hydrothermal synthesis of WO_3 nanorods and their sensing properties for NO_2", *J. Mater. Chem.*, **22** [25] (2012) 12643–12650.
112. T. Kida, A. Nishiyama, Z. Hua, K. Suematsu, M. Yuasa, K. Shimanoe, "WO_3 nanolamella gas sensor: Porosity control using SnO_2 nanoparticles for enhanced NO_2 sensing", *Langmuir*, **30** [9] (2014) 2571–2579.
113. C. Wang, C. Feng, M. Wang, X. Li, P. Cheng, H. Zhang, Y. Sun, P. Sun, G. Lu, "One-pot synthesis of hierarchical WO_3 hollow nanospheres and their gas sensing properties", *RSC Adv.*, **5** [38] (2015) 29698–29703.
114. I. Aslam, C. Cao, M. Tanveer, W.S. Khan, M. Tahir, M. Abid, F. Idrees, F.K. Butt, Z. Ali, N. Mahmood, "The synergistic effect between WO_3 and g-C_3N_4 towards efficient visible-light-driven photocatalytic performance", *New J. Chem.*, **38** [11] (2014) 5462–5469.
115. C. Shifu, J. Lei, T. Wenming, F. Xianliang, "Fabrication, characterization and mechanism of a novel Z-scheme photocatalyst $NaNbO_3$/WO_3 with enhanced photocatalytic activity", *Dalt. Trans.*, **42** [30] (2013) 10759–10768.
116. N. Vorobyeva, M. Rumyantseva, D. Filatova, E. Konstantinova, D. Grishina, A. Abakumov, S. Turner, A. Gaskov, "Nanocrystalline ZnO(Ga): Paramagnetic centers, surface acidity and gas sensor properties", *Sensor. Actuat. B Chem.*, **182** (2013) 555–564.
117. P.G. Su, T.T. Pan, "Fabrication of a room-temperature NO_2 gas sensor based on WO_3 films and WO_3/MWCNT nanocomposite films by combining polyol process with metal organic decomposition method", *Mater. Chem. Phys.*, **125** [3] (2011) 351–357.
118. W. Yan, M. Hu, P. Zeng, S. Ma, M. Li, "Room temperature NO_2-sensing properties of WO_3 nanoparticles/porous silicon", *Appl. Surf. Sci.*, **292** (2014) 551–555.
119. U. Yaqoob, A.S.M.I. Uddin, G.S. Chung, "A high-performance flexible NO_2 sensor based on WO_3 NPs decorated on MWCNTs and RGO hybrids on PI/PET substrates", *Sensor. Actuat. B Chem.*, **224** (2016) 738–746.
120. P.G. Su, S.L. Peng, "Fabrication and NO_2 gas-sensing properties of reduced graphene oxide/WO_3 nanocomposite films", *Talanta*, **132** (2015) 398–405.
121. Y. Wei, M. Hu, W. Yan, D. Wang, L. Yuan, Y. Qin, "Hydrothermal synthesis porous silicon/tungsten oxide nanorods composites and their gas-sensing properties to NO_2 at room temperature", *Appl. Surf. Sci.*, **353** (2015) 79–86.